Synchronization of Cyclic Power Grids
Equilibria and Stability of the Synchronous State

Xi, Kaihua; Dubbeldam, Johan; Lin, Hai Xiang

DOI
10.1063/1.4973770

Publication date
2017

Document Version
Final published version

Published in
Chaos: an interdisciplinary journal of nonlinear science

Citation (APA)
Xi, K., Dubbeldam, J., & Lin, H. X. (2017). Synchronization of Cyclic Power Grids: Equilibria and Stability of the Synchronous State. *Chaos: an interdisciplinary journal of nonlinear science*, *27*(1), 1-11. Article 013109. https://doi.org/10.1063/1.4973770

Synchronization of cyclic power grids: Equilibria and stability of the synchronous state

Kaihua Xi, Johan L. A. Dubbeldam, and Hai Xiang Lin

Citation: Chaos **27**, 013109 (2017);
View online: https://doi.org/10.1063/1.4973770
View Table of Contents: http://aip.scitation.org/toc/cha/27/1
Published by the American Institute of Physics

Synchronization of cyclic power grids: Equilibria and stability of the synchronous state

Kaihua Xi,[a] Johan L. A. Dubbeldam,[b] and Hai Xiang Lin[c]
Delft Institute of Applied Mathematics, Delft University of Technology, Mekelweg 4, 2628 CD Delft, The Netherlands

(Received 29 July 2016; accepted 26 December 2016; published online 11 January 2017)

Synchronization is essential for the proper functioning of power grids; we investigate the synchronous states and their stability for cyclic power grids. We calculate the number of stable equilibria and investigate both the linear and nonlinear stabilities of the synchronous state. The linear stability analysis shows that the stability of the state, determined by the smallest nonzero eigenvalue, is inversely proportional to the size of the network. We use the energy barrier to measure the nonlinear stability and calculate it by comparing the potential energy of the type-1 saddles with that of the stable synchronous state. We find that the energy barrier depends on the network size (N) in a more complicated fashion compared to the linear stability. In particular, when the generators and consumers are evenly distributed in an alternating way, the energy barrier decreases to a constant when N approaches infinity. For a heterogeneous distribution of generators and consumers, the energy barrier decreases with N. The more heterogeneous the distribution is, the stronger the energy barrier depends on N. Finally, we find that by comparing situations with equal line loads in cyclic and tree networks, tree networks exhibit reduced stability. This difference disappears in the limit of $N \to \infty$. This finding corroborates previous results reported in the literature and suggests that cyclic (sub)networks may be applied to enhance power transfer while maintaining stable synchronous operation. *Published by AIP Publishing.* [http://dx.doi.org/10.1063/1.4973770]

The electrical power grid is a fundamental infrastructure in today's society and synchronization is essential for the proper functioning of the power grid. The current transition to a more distributed generation of energy by renewable sources, which are inherently more prone to fluctuations, poses even greater challenges to the functioning of the power grid. As the contribution of renewable energy to the total power being generated is surging, it becomes more challenging to keep the synchronization against large disturbances. The objective of this paper is to study the influence of cycles in the network, and of the distribution of power generation and consumption, on the synchronization. We find that the heterogeneity of power generation and consumption diminishes both the linear stability and the nonlinear stability and that large size cyclic power grids are more sensitive to this heterogeneity. In addition, we show that a line in a tree network loses synchronization more easily than a line carrying the same amount of power in a ring network. This suggests that the stability of the synchronous state can be improved by forming small cycles in the network. The findings may help optimize the power flow and design the topology of future power grids.

I. INTRODUCTION

In power grids, the topology of the network and the distribution of power generation and consumption play important roles in the synchronization.[1–8] The linear stability of the synchronized state against small size disturbances has been widely studied using the master stability formalism of Pecora and Carroll,[9] e.g., Refs. 2, 5, 7, and 8. Complementary work on large disturbances was described by Menck *et al.*[5] with the concept of *basin stability*, which was applied to estimate the basin of attraction of the synchronous state. In practice, the significance of stable operation of the power grid was acknowledged long ago and has led to general stability studies for the power grid using *direct methods*,[10–12] which focus on the potential energy landscape of nonlinear power systems.

The primary interest of this paper is to study the influence of cycles and of the distribution of generators and consumers on the synchronization. In particular, we study cyclic power grids to analyze the impact of the size of the cycle and of the heterogeneity of the power distribution on the synchronization.

We focus on the potential energy landscape of the nonlinear systems and use the *energy barrier* to measure the nonlinear stability. The energy barrier prevents loss of synchronization and is defined as the potential energy difference between the type-1 equilibria and the corresponding stable equilibrium. Starting from the commonly used second-order swing equations, we reduce our model to a system of first-order differential equations using the techniques developed by Varaiya and Chiang[10,13] to find stability regions for synchronous operation of electric grids after a contingency. After this reduction, we are left with a first-order Kuramoto model with nearest neighbor coupling.

For the case of a cyclic power grid with a homogeneous distribution of power generation and consumption, we derive analytical expressions for the stable equilibria and for their

[a]Electronic mail: K.Xi@tudelft.nl
[b]Electronic mail: j.l.a.dubbeldam@tudelft.nl
[c]Electronic mail: H.X.Lin@tudelft.nl

number, which generalize earlier work of DeVille.[14] Furthermore, we investigate the more general case with random distributions of generators and consumers numerically. To this end, we develop a novel algorithm that allows fast determination of the stable equilibria, as well as the saddle points in the system.

Subsequently, the stability of the equilibria is studied both using linearization techniques for linear stability and direct (energy) methods for determining the nonlinear stability. By comparing our stability results for different network sizes, we show that the linear stability properties differ greatly from the energy barrier obtained by direct methods when the system size increases. More specifically, the linear stability measured by the first nonzero eigenvalue approximately scales with the number of nodes (N) as $1/N$. This is consistent with the findings by Lu *et al.*[15] on the linear stability of a chain or cyclic network. However, this is in contrast to the nonlinear stability result in this study, which shows that the potential energy barrier decreases to a nonzero value for $N \to \infty$. For large size cyclic power grids, small perturbations of the power supply or consumption may lead to desynchronization. Moreover, comparison of a ring topology with a tree topology reveals enhanced stability for the ring configuration. This result suggests that the finding that dead-ends or dead-trees diminish stability by Menck *et al.*[5] can be interpreted as a special case of the more general fact that tree-like connection desynchronizes easier than ring-like connection. This confirms the earlier result in Refs. 16 and 17 that forming small cycles can increase the stability of the synchronous state. However, it does not mean that stability can be increased by arbitrary adding more cycles in the network because of the well-known *Braess' paradox*, which has also been found in power systems.[6,7] In this situation, the stability of the synchronous state decreases after the introduction of additional lines to the network. Hence, when a cycle is added to the network to improve the stability, the Braess's paradox should be avoided.

In this paper, we focus on the linear and nonlinear stabilities of cyclic power grids. The paper is organized as follows. We define the model in Section II and calculate the (number of) stable equilibria of cyclic networks in Section III. We next analyze the linear stability of the synchronous states in Section IV and the nonlinear stability in Section V. Finally, we conclude with a summary of our results in Section VI.

II. INTRODUCTION OF THE MODEL

We consider the second order Kuramoto model defined by the following differential equations:

$$\frac{d^2\delta_i}{dt^2} + \alpha\frac{d\delta_i}{dt} + K\sum_j A_{ij}\sin\left(\delta_i - \delta_j\right) = P_i, \tag{1}$$

where the summation is over all N nodes in the network. In Eq. (1) δ_i is the phase of the $i-$th generator/load and P_i is the power that is generated ($P_i > 0$) or consumed ($P_i < 0$) at node i and $\alpha > 0$ is the damping parameter that we take equal for all nodes. The link or coupling strength is denoted by K and A_{ij} is the coefficient in the adjacency matrix of the network. The model also is called the second-order Kuramoto model, see, e.g., Refs. 2, 5, and 18–20.

When we consider the case of a ring network, Eq. (1) reduces to

$$\frac{d^2\delta_i}{dt^2} + \alpha\frac{d\delta_i}{dt} + K\left[\sin(\delta_i - \delta_{i+1}) + \sin(\delta_i - \delta_{i-1})\right] = P_i, \tag{2}$$

with $i = 1, 2, \ldots, N$. In writing Eq. (2), we assumed that $\delta_{N+i} = \delta_i$. We usually rewrite the second-order differential equations as the first-order system

$$\begin{aligned}\dot{\delta}_i &= \omega_i,\\ \dot{\omega}_i &= P_i - \alpha\omega_i - K[\sin(\delta_i - \delta_{i+1}) + \sin(\delta_i - \delta_{i-1})].\end{aligned} \tag{3}$$

Note that in an equilibrium, the total consumption equals to the total amount of generation, i.e., $\sum_{i=1}^{N} P_i = 0$.

The *line load* of a line is defined as follows:

$$\mathcal{L}_{i,j} = K|\sin(\delta_i - \delta_j)|, \tag{4}$$

which measures the power transmitted by the line connecting node i and node j.

In this paper, we focus on the power distribution with the form

$$\begin{aligned}P_i &= (-1)^{i+1}P + \xi_i, \quad i = 1, 2, \ldots, N-1.\\ \xi_i &\in N(0,\sigma), \text{ and } \sum_{i=1}^{N} P_i = 0,\end{aligned} \tag{5}$$

where $N(0,\sigma)$ is the normal distribution with standard deviation $\sigma \geq 0$ and mean 0, and ξ_i is a random number. We refer the model with $\sigma = 0$ as the *homogeneous model* in which power P is generated at the odd nodes and $-P$ is consumed at the even nodes, i.e.,

$$P_i = (-1)^{i+1}P. \tag{6}$$

Further, we refer the model with $\sigma > 0$ as the *heterogeneous model*, which is obtained by a Gaussian perturbation of the homogeneous model. The degree of heterogeneity of P_i in the heterogeneous model is measured by σ.

To investigate the linear stability of the synchronous (equilibrium) state, Eq. (3) are linearized around an equilibrium state $(\delta_i^s, 0)$, $i = 1, \ldots, N$. Using vector notation $\boldsymbol{\delta} = (\delta_1, \ldots, \delta_N)^T$ and $\boldsymbol{\omega} = (\omega_1, \ldots, \omega_N)^T$, the linearized dynamics is given by the matrix differential equation

$$\begin{pmatrix}\dot{\boldsymbol{\delta}}\\ \dot{\boldsymbol{\omega}}\end{pmatrix} = \begin{pmatrix}0 & I_N\\ L & -\alpha\end{pmatrix}\begin{pmatrix}\boldsymbol{\delta}\\ \boldsymbol{\omega}\end{pmatrix} = J\begin{pmatrix}\boldsymbol{\delta}\\ \boldsymbol{\omega}\end{pmatrix}, \tag{7}$$

with L the (negative) Laplacian matrix defined by

$$\begin{aligned}L_{i,i-1} &= K\cos(\delta_i - \delta_{i-1}),\\ L_{i,i+1} &= K\cos(\delta_i - \delta_{i+1}),\\ L_{i,i} &= -K[\cos(\delta_i - \delta_{i-1}) + \cos(\delta_i - \delta_{i+1})].\end{aligned} \tag{8}$$

The eigenvalues of L, denoted by λ_i, are related to the eigenvalues of J, denoted by μ_i, according to the following equation:

$$\mu_{i\pm} = -\frac{\alpha}{2} \pm \frac{1}{2}\sqrt{\alpha^2 + 4\lambda_i}, \quad i = 1, 2, \ldots, N-1. \tag{9}$$

These $2N-2$ eigenvalues are supplemented by two eigenvalues 0; one corresponding to a uniform frequency shift and the other to a uniform phase shift. For $\alpha > 0$, the real part of $\mu_{i\pm}$ is negative if $\lambda_i < 0$. The *type-j equilibria* are defined as the ones whose Jacobian matrix J have j eigenvalues with a positive real part.

III. THE EQUILIBRIA OF RING NETWORKS

In this section, we study a ring network consisting of an even number of nodes (N) with $N/2$ generators and $N/2$ consumers, e.g., as shown in Fig. 1. The phase differences between neighbors are

$$\theta_1 \equiv \delta_1 - \delta_N (\mathrm{mod}\ 2\pi), \quad \theta_{i+1} \equiv \delta_{i+1} - \delta_i (\mathrm{mod}\ 2\pi).$$

To find the equilibrium points we set $(\delta_i, \dot{\delta}_i) = (\delta^s, 0)$ in Eq. (3) from which we find the following equations for θ_i:

$$\sin\theta_i - \sin\theta_{i+1} = P_i/K, \qquad i = 1, \ldots, N. \tag{10}$$

Because all phase differences θ_i are restricted to one period of θ_i, the following additional requirement holds:

$$\sum_{i=1}^{N} \theta_i = 2m\pi, \ m \in \{-\lfloor N/2 \rfloor, \ldots, -1, 0, 1, \ldots, \lfloor N/2 \rfloor\}, \tag{11}$$

where $\lfloor N/2 \rfloor$ denotes the floor value of $N/2$, that is, the largest integer value which is smaller than or equal to $N/2$. Each equilibrium corresponds to a synchronous state whose stability we wish to determine. We first calculate the number of stable equilibria of the homogeneous model. Note that these equilibria correspond to phase-locked solutions of a first-order Kuramoto model that was explored by DeVille[14] for the case $P = 0$.

A. The equilibria of the homogeneous model

In this subsection, the number of stable equilibria is determined by solving the nonlinear system analytically. Our approach is similar to that of Ochab and Góra.[21] Note that for general ring networks, an upper bound of the number of stable equilibria has been derived by Delabays *et al.*,[22] which is a linear function of the size N. Here, we focus on the special case with the homogeneous model as described in Eq. (6), we have the following proposition.

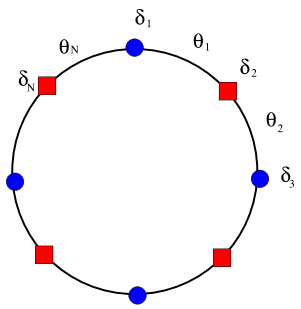

FIG. 1. A ring network with alternating consumer and generator nodes. Circle nodes are generators and square nodes are consumers.

Proposition III. 1. *The equilibria of the ring network with homogeneous distribution of generation and consumption as in Eq. (6) are given by* $\theta_i = \theta_1$ *for odd* i, *and* $\theta_i = \theta_2$ *for even* i, *where*

$$\theta_1 = \arcsin\left[\frac{P}{2K\cos\frac{2m\pi}{N}}\right] + \frac{2\pi m}{N}, \tag{12a}$$

$$\theta_2 = -\arcsin\left[\frac{P}{2K\cos\frac{2m\pi}{N}}\right] + \frac{2\pi m}{N}, \tag{12b}$$

and m is an integer such that

$$|m| \le \left\lfloor \frac{N}{2\pi} \arccos\left(\sqrt{\frac{P}{2K}}\right) \right\rfloor.$$

The total number of stable equilibria is given by

$$N_s = 1 + 2\left\lfloor \frac{N}{2\pi} \arccos\left(\sqrt{\frac{P}{2K}}\right) \right\rfloor. \tag{13}$$

When $P = 0$, N_s reaches the upper bound derived in Ref. 22. Details of this derivation can be found in supplementary material Section S1.

In the following, we denote the stable equilibria as $\boldsymbol{\theta}_S^m = (\theta_1^m, \theta_2^m, \ldots, \theta_1^m, \theta_2^m)$ where θ_1^m, θ_2^m can be calculated by Eq. (12).

In Fig. 2(a), we show the total number of stable equilibria N_S as a function of P/K. It can be clearly seen from this figure that the total number of stable equilibria decreases with P/K and reaches 0 when $P/K = 2$.

B. The equilibria of the heterogeneous model

To investigate the effect of the distribution of P_i, we performed Monte Carlo (MC) simulations of the system (3) with the distribution of P_i given by Eq. (5).

All the equilibria of small size power systems can be found using a software package Bertini.[23–25] However, we perform numerical calculations using the algorithm in supplementary material Section S2 since the size of the networks is relatively large. The algorithm amounts to finding all solutions for β of

$$\sum_{i=1}^{N} a_i \arcsin\left(\sum_{j=1}^{i} P_j/K + \beta\right) = m\pi,$$

where $a_i = 1$ when the phase difference $\theta_i \in [-\pi/2, \pi/2]$ and $a_i = -1$ if $\theta_i \in [\pi/2, 3\pi/2]$. For details and bounds on the values of m, we refer to supplementary material Section S2. Since the number of equilibria is known to increase exponentially with N,[26,27] it is not feasible to find all equilibria for large networks. Therefore, we developed an algorithm based on a recent theoretical paper of Bronski and DeVille[28] for finding all equilibria of type-j. Details about the algorithm can be found in supplementary material Section S2. We are particularly interested in type-1 equilibria, as a union of the stable manifolds of these equilibria can be used to

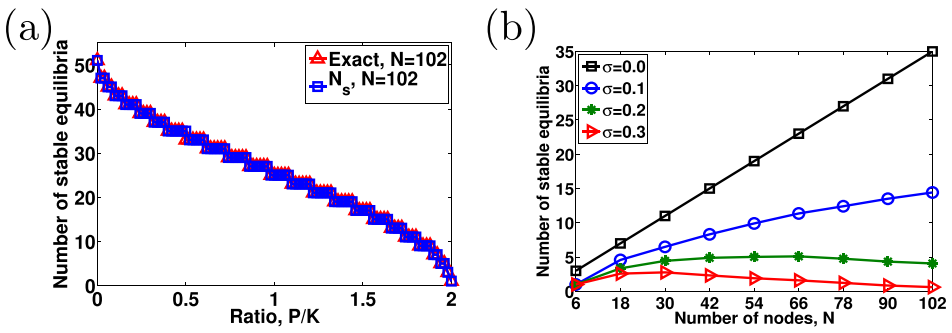

FIG. 2. (a) The number of stable equilibria according to Eq. (13) compared to the numerically calculated number of stable equilibria. (b) The number of stable equilibria as a function of N, $P/K = 0.5$. With a larger σ, it becomes more difficult for the power system to synchronize to a stable state.

approximate the basin of stability of the stable equilibria. Our algorithm is capable to find type-1 equilibria at a computational cost of $O(N^3)$ and hence can be applied to rather large networks. We remark that this algorithm might be extended to more general networks. Employing this algorithm, the number of stable equilibria is investigated as follows.

Our algorithm was applied to networks with $P/K = 0.5$ described by the heterogeneous model. In the simulations, we average over 1000 independent runs for each value of σ. In Fig. 2(b), the number of stable equilibria is plotted as a function of the number of nodes that we vary from $N = 6$ to $N = 102$, for 4 different values of $\sigma = 0$, 0.1, 0.2, and 0.3. It can clearly be seen that for $\sigma = 0.2$ or $\sigma = 0.3$ the number of stable equilibria attains a maximum value and then decreases. The same behavior is also expected for $\sigma = 0.1$. However, the decrease is expected to set in at larger values of N; hence, such behavior cannot be observed from Fig. 2(b). The occurrence of a maximum for nonzero σ can be understood as follows. If the number of nodes increases, the probability that a phase difference between two nodes exceeds $\pi/2$ also increases. Even though for moderately large N ($1 < N < 50$), the fact that more equilibria can be found increases linearly with N, as was shown in Eq. (13), this increase is much smaller than the decrease caused by the arising probability of phase differences beyond $\pi/2$. This may be explained by the fact that in larger networks the probability to form clusters in which neighboring nodes i and $i+1$ have large $\Delta P = |P_i - P_{i+1}|$ increases more rapidly than linearly with N. As a larger ΔP is associated with larger phase differences, such clusters with large fluctuations in ΔP between its members are likely to result in asynchronous behavior. This finding is in agreement with the well-known result that no synchronous states exist for an infinite Kuramoto network; see also Ref. 29.

Note that for a certain distribution of P_i, equilibria can be found with at least one phase difference exceeding $\frac{\pi}{2}$, but nevertheless being stable. This is in accordance with the graph theoretical result of Bronski and DeVille[28] and numerical findings of Mehta *et al.*[23]

IV. LINEAR STABILITY OF EQUILIBRIA

To determine the stability of the equilibria, the eigenvalues of the matrix corresponding to the system of second-order differential equations are required. These can be calculated analytically for single generator coupled to an infinite bus system for any value of damping parameter α, in which case the system is described by a single second-order differential equation. Such an approach was also taken by Rohden *et al.*[2,19]

The eigenvalues of the linearized system Eq. (7) can be explained in forms of the eigenvalues of L as shown in Eq. (9). Thus, the stability of equilibrium is determined by the eigenvalues of L, i.e., a positive eigenvalue λ_i of L results in a corresponding eigenvalue μ_i with positive real part.[30]

We focus on the stable equilibrium with all eigenvalues of L negative and all $N-1$ pairs of eigenvalue in Eq. (9) are complex valued with negative real part. The most stable situation arises when the damping coefficient α is tuned to the optimal value α_{opt} described by Motter *et al.*:[8] $\alpha_{\text{opt}} = 2\sqrt{-\lambda_1}$, where λ_1 is the least negative eigenvalue of L, in that case $\mu_1 = -\sqrt{-\lambda_1}$. So the linear stability of the power grid is governed by the eigenvalues of L, which is further investigated in this section.

The entries of the matrix L that arises after linearization around the synchronized state $(\boldsymbol{\delta}^s, \mathbf{0})$ are easily calculated and from that we find that L is the following Laplacian matrix:

$$L = \begin{pmatrix} -c_2 - c_1 & c_2 & 0 & \cdots & 0 & c_1 \\ c_2 & -c_2 - c_3 & c_3 & 0 & \cdots & 0 \\ 0 & \ddots & \ddots & \ddots & \ddots & 0 \\ 0 & \cdots & 0 & c_{N-2} & -c_{N-2} - c_{N-1} & c_{N-1} \\ c_1 & 0 & \cdots & 0 & c_{N-1} & -c_1 - c_{N-1} \end{pmatrix}, \tag{14}$$

where $c_i = K\cos(\delta_i - \delta_{i-1}) = K\cos\theta_i$. As matrix L is a (symmetric) Laplacian matrix with zero-sum rows, $\lambda = 0$ is an eigenvalue. This reflects a symmetry in the system: if all phases are shifted by the same amount β, the system of differential equations remains invariant. It is well known that when all entries $c_i > 0$, L is negative definite; hence, all eigenvalues are non-positive, which implies stable equilibria with the phase differences $|\delta_i - \delta_{i-1}| \leq \pi/2 \pmod{2\pi}$, for all $i = 1, \ldots, N$.

A. The linear stability of the homogeneous model

For the homogeneous model, we derive a theorem which shows that type-1 equilibria appear if a single phase difference between two nodes has negative cosine value and type-j equilibria with $j > 1$ appear if more than one phase differences have a negative cosine value. In the following, we write a phase difference exceeds $\pi/2 \pmod{2\pi}$ if it has a negative cosine value. We summarize our findings in the

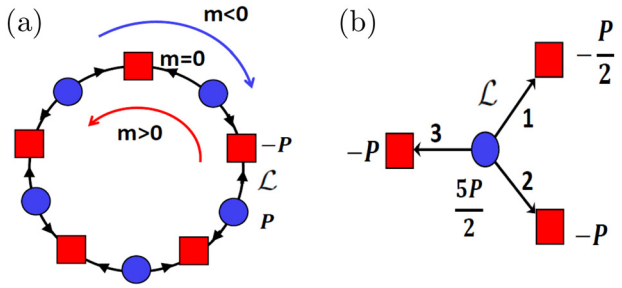

FIG. 3. (a) A cyclic power grid with alternating consumers and generators, which may have stable equilibria with the power transported around the cycle clockwise with $m<0$ and counterclockwise with $m>0$. The practical synchronization state is the one with $m=0$, in which the line load $\mathcal{L}=P/2$. (b) A tree power grid with 3 nodes. The line load of line 1 $\mathcal{L}=P/2$.

following theorem, which slightly generalizes similar results obtained in Refs. 14 and 31.

Theorem IV. 1. *All stable equilibria of a power grid with ring topology and homogeneous distribution of power consumption and generation as described in Eq. (6) are given by Eq. (12). Stability of the synchronous states in the network, corresponding to negative eigenvalues of the matrix J, is guaranteed as long as* $|\delta_i-\delta_{i-1}|\le\pi/2\,(\mathrm{mod}\,2\pi)$. *If a single phase difference exceeds* $\pi/2\,(\mathrm{mod}\,2\pi)$ *this synchronous state turns unstable and the corresponding equilibrium is type-1. Moreover, synchronized states with more than one absolute phase difference exceeding* $\pi/2\,(\mathrm{mod}\,2\pi)$ *correspond to equilibria with at least two unstable directions, that is, to type-j equilibria with* $j>1$.

The proof of the theorem can be found in supplementary material Section S1.

Theorem IV.1 confirms that Eq. (12) indeed capture all the stable equilibria of the homogeneous model, on which we make two remarks on the homogeneous model.

Remark I. We notice that for the case $N\equiv 0\,(\mathrm{mod}\,4)$ an infinite number of equilibria exist for the homogeneous model. We will not consider this nongeneric case here, but refer to the work of DeVille[14] for more details about this case.

Remark II. The stable equilibria depend on m. For practical purposes the case $m=0$ is most desirable for transport of electricity, as in this case direct transport of power from the generator to the consumer is realized. Direct transport from generator to consumer minimizes energy losses that always accompany the transport of electrical power. The power is transported clockwise if $m<0$ and counterclockwise if $m>0$ as shown in Fig. 3(a). Note that the loop flows of the equilibria with $m\neq 0$ may exist in general networks with cycles, see Refs. 22 and 32 for more details.

For the case $m=0$, the stable equilibrium is $\boldsymbol{\theta}_S=(\theta_1,\theta_2,\ldots,\theta_N)$ with $\theta_1=-\theta_2=\arcsin\left[\frac{P}{2K}\right]$ as follows from Eq. (12). It is interesting to explore the ramifications of our results for the eigenvalues of L of the second-order model. We write the eigenvalues of the matrix L that result after linearizing around the stable state (12) with $m=0$, which can easily be determined

$$\lambda_n=-2\sqrt{4K^2-P^2}\sin^2\left(\frac{\pi n}{N}\right),\quad n=0,1,\ldots,N-1. \tag{15}$$

The first nonzero eigenvalue, $\lambda_1=-2\sqrt{4K^2-P^2}\sin^2(\pi/N)$, gives rise to an associated eigenvalue pair for matrix J

$$\begin{aligned}\mu_{1,+}&=\frac{-\alpha}{2}+\frac{\sqrt{\alpha^2-8\sin^2(\pi/N)\sqrt{4K^2-P^2}}}{2},\\ \mu_{1,-}&=\frac{-\alpha}{2}-\frac{\sqrt{\alpha^2-8\sin^2(\pi/N)\sqrt{4K^2-P^2}}}{2},\end{aligned} \tag{16}$$

whose optimal value is obtained if α is tuned to the value which makes the square root vanish.[8] For this value of α, $\mu_{1,+}=\mu_{1,-}=\mu_{\mathrm{opt}}$, which equals

$$\mu_{\mathrm{opt}}=-\sqrt{-\lambda_1}=-(4K^2-P^2)^{1/4}\sqrt{2}\sin(\pi/N). \tag{17}$$

From Eq. (17), we easily observe that μ_{opt} increases to 0 with a rate of $1/N$ for N sufficiently large. This suggests that networks with many nodes are much more susceptible to perturbations; hence, it is more difficult for the power grid to remain synchronized.

B. The linear stability of the heterogeneous model

To investigate the effect of more heterogeneous distribution of power generation and consumption, we determine the linear stability of the stable equilibria found using the numerical algorithm described in supplementary material Section S2. We perform MC simulations to generate heterogeneous distributions of power generation and consumption using the method given in Eq. (5), and average over 1000 runs. In all runs, we set $P=1$ and $K=8$, so $P/K=0.125$. In Fig. 4(a), we plotted the value of $-\mu_{\mathrm{opt}}$ for two values of σ as a function of N. Indeed the dependence on N is as predicted, and the two curves almost coincide, which means that the eigenvalue is not so sensitive to the heterogeneity of power distribution for the setting of P and K. In Fig. 4(b), we explore the dependence on σ. Here, we see as the heterogeneity of P_i increases, the expected linear stability decreases. However, only a very mild dependence on σ can be seen, so the heterogeneity does not seem to be very important for this value of P/K. To better understand how each configuration of consumers and generators rather than the averaged configuration changes its stability with increasing heterogeneity, we plotted the distribution of $-\mu_{\mathrm{opt}}$ in Figs. 4(c) and 4(d). These show that besides a small shift of the maximum toward smaller values of $-\mu_{\mathrm{opt}}$ the distribution is also broader, which indicates that certain configuration will be less stable than others. We remark that the value of the y axis is relatively large, which means that the $-\mu_{\mathrm{opt}}$ is very close to the average value.

V. NONLINEAR STABILITY OF THE SYNCHRONOUS STATE IN RING NETWORKS

We next discuss the stability of synchronous operation when the system is subject to perturbations of such a degree that render the linear stability analysis of Section IV inappropriate. A measure for the stability of the stationary states is then provided by the basin of attraction of the equilibria. For high-dimensional systems, this is a daunting task. However, it is possible to estimate the volume of the basin either by numerical techniques, such as for example, the recently introduced

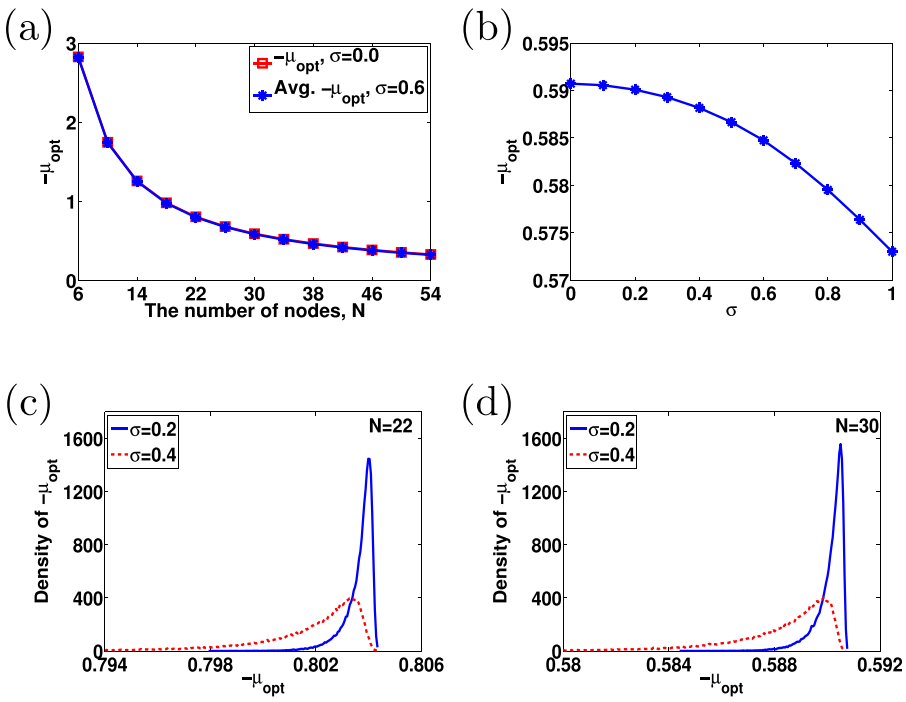

FIG. 4. (a) $-\mu_{\text{opt}}$ as a function of N for $\sigma = 0$ and $\sigma = 0.6$. (b) $-\mu_{\text{opt}}$ as a function of σ with $N = 30$. (c) The distribution of $-\mu_{\text{opt}}$ for $\sigma = 0.2$ and $\sigma = 0.4$ and $N = 22$. (d) The density of $-\mu_{\text{opt}}$ for $\sigma = 0.2$ and $\sigma = 0.4$ where $N = 30$. $P/K = 0.125$ is kept fixed in all panels.

basin stability S, by Menck *et al.*,[5,33] in which the phase space is divided into small volumes. Choosing initial conditions in each of the small volumes and recording convergence to a stable equilibrium for each attempted initial condition, a number S between 0 and 1, which is a measure for the size of the volume of the attracting phase space, can be obtained. Since this technique is computationally demanding and also labels solutions which make large excursions through phase space as stable,[34] as they do belong to the stable manifold of the equilibrium, we will follow a different approach.

The stability region has been analyzed by Chiang[35] and independently Zaborszky *et al.*[30,36] and the direct method was developed by Varaiya *et al.*[10,13] to find a conservative approximation to the basin of stability. The approximation actually is the minimal energy barrier, which prevents loss of synchronization.

Here, we measure the nonlinear stability by the energy barrier. We define an energy function $E(\boldsymbol{\delta}, \boldsymbol{\omega})$ by

$$\begin{aligned} E(\boldsymbol{\delta}, \boldsymbol{\omega}) &= \frac{1}{2}\sum_{i=1}^{N}\omega_i^2 - \sum_{i=1}^{N}P_i\delta_i - K\sum_{i=1}^{N}(\cos(\delta_{i+1} - \delta_i)), \\ &= \frac{1}{2}\sum_{i=1}^{N}\omega_i^2 + V(\boldsymbol{\delta}), \end{aligned} \tag{18}$$

where the potential $V(\boldsymbol{\delta})$ is

$$V(\boldsymbol{\delta}) = -K\sum_{i=1}^{N}\cos(\delta_{i+1} - \delta_i) - \sum_{i=1}^{N}P_i\delta_i. \tag{19}$$

It can easily be shown that

$$\frac{dE(\boldsymbol{\delta}, \boldsymbol{\omega})}{dt} = -\alpha\sum_{i=1}^{N}\omega_i^2 \leq 0.$$

The primary idea behind estimating the region of attraction of a stable equilibrium by the direct method is that this region is bounded by a manifold $\mathcal{M}$ of the type-1 equilibria that reside on the *potential energy boundary surface* (PEBS) of the stable equilibrium. The PEBS can be viewed as the stability boundary of the associated gradient system[10,12]

$$\frac{d\delta_i}{dt} = -\frac{\partial V(\boldsymbol{\delta})}{\partial \delta_i}. \tag{20}$$

The *closest equilibrium* is defined as the one with the lowest potential energy on the PEBS.[37,38] By calculating the closest equilibrium with potential energy $V_{\min}$ and equating this to the total energy, it is guaranteed that points within the region bounded by the manifold $\mathcal{M} = \{(\delta, \omega) | E(\delta, \omega) = V_{\min}\}$ will always converge to the stable equilibrium point contained in $\mathcal{M}$.

The idea of estimating the region of stability by type-1 equilibria is probably best illustrated by considering a simple example of a three-node network depicted in Fig. 5(a). We choose this network only for illustration purposes as this small three-node network allows direct evaluation. For this network, we set $P_1/K = 0.125, P_2 = -0.125, P_3/K = 0$ and $\alpha = 0$. Equipotential curves are plotted in Fig. 5(b). The type-1 equilibria (saddles) are displayed as little stars and pentagrams, numbered 1–6. It is clear that the type-1 equilibria indeed surround the stable equilibria which are shown as local minima in the potential V. Equilibrium 1 is the closest equilibrium with the smallest potential energy on the PEBS plotted by a black dashed-dotted line. A small perturbation in the direction to saddle point 1, depicted by the red dashed curve, leads to desynchronization, whereas a larger perturbation in a different direction (blue solid curve) eventually decays toward the stable equilibrium point and hence the system stays synchronized. This shows the conservativity of the direct method and the challenges in calculating the region of stability, as it depends on both the direction and size of the perturbation. One approach to this problem is to

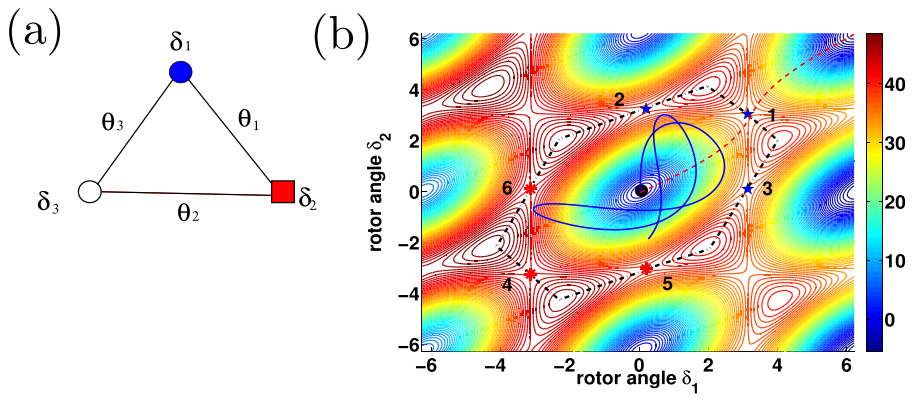

FIG. 5. (a) A 3-node power grid with $P_1/K = 0.125, P_2/K = -0.125$ and $P_3/K = 0$, and $\theta_1 = \delta_1 - \delta_2$, $\theta_2 = \delta_2 - \delta_3$, $\theta_3 = \delta_3 - \delta_1$. (b) The potential energy as a function of δ_1 and δ_2, where $\delta_3 = 0$. The 6 unstable equilibria are local minima on the potential energy boundary surface (PEBS) plotted by the black dashed-dotted line. The equilibria 1 and 4 correspond to the cases that θ_1 exceeds $\pi/2$ and $-\pi/2$, respectively. Similarly, the equilibria 2 and 5 correspond to the cases that θ_2 exceeds $-\pi/2$ and $\pi/2$, respectively, and the equilibria 3 and 6 correspond to the cases that θ_3 exceeds $-\pi/2$ and $\pi/2$, respectively. Equilibrium 1 is the closest equilibrium. The trajectory plotted by the red dashed line goes through equilibrium 1 and results in desynchronization after θ_1 exceeds $\pi/2$. However, the trajectory plotted by the blue solid line always stays inside the attraction of the stable equilibrium in the middle even though its energy is larger than the potential energy of equilibrium 1.

determine the so-called *controlling unstable equilibrium*, e.g., Chiang *et al.*[11,35] We will not consider this method here, but rather restrict ourselves to the potential energy of all the type-1 saddles on the PEBS, to the energy barriers in special which are the potential energy differences between the type-1 saddles and the stable equilibrium. As displayed in Fig. 5(b), there are two type-1 saddles corresponding to the absolute value $|\theta_i|$ of a phase difference exceeding $\pi/2$. The potential energy of these two saddles is different and the one with smaller potential energy is more susceptible to perturbations. In the following study, all the equilibria are divided into two groups: (I) a group that corresponds to $|\theta_i|$ exceeding $\pi/2$ with smaller energy and (II) the other group with larger energy. In Fig. 5(b), direct calculation shows that the saddles (1–3) constitute group I and (4–6) constitute group II.

We remark that closest equilibrium 1 corresponds to the line connecting node 1 and 2 with the largest line load. This makes sense since the line with higher line load is easier to lose synchronization first.

In Subsection V A, we derive the analytical approximation of energy barriers of the homogeneous model, for group I and group II, respectively. In Subsection V B, we present the numerical results for the heterogeneous model.

A. Potential energy for the homogeneous model

The potential energy of the stable state $\boldsymbol{\theta}_S^m$ derived by Eq. (12) is

$$\begin{aligned} V_S^m &= -K\sum_{i=1}^{N}\cos\left(\theta_i^m\right) - \sum_{i=1}^{N}P(-1)^{i+1}\delta_i, \\ &= -\frac{KN}{2}\left[\cos\left(\theta_1^m\right)+\cos\left(\theta_2^m\right)\right] + \frac{NP}{4}\left[\theta_2^m - \theta_1^m\right]. \end{aligned} \tag{21}$$

We next consider the potential energy of the type-1 saddle points. According to Theorem IV.1, a type-1 saddle point corresponds to a link with absolute phase difference exceeding $\pi/2\,(\mathrm{mod}\,2\pi)$ in the network. We denote the type-1 saddle points corresponding to the stable state $\boldsymbol{\theta}_S^m$ by

$$\boldsymbol{T}_j^m = \left(\hat{\theta}_1^m, \hat{\theta}_2^m, \ldots, \pi - \hat{\theta}_1^m, \hat{\theta}_2^m, \ldots, \hat{\theta}_1^m, \hat{\theta}_2^m\right)$$

and

$$\bar{\boldsymbol{T}}_j^m = \left(\hat{\theta}_1^m, \hat{\theta}_2^m, \ldots, -\pi - \hat{\theta}_1^m, \hat{\theta}_2^m, \ldots, \hat{\theta}_1^m, \hat{\theta}_2^m\right),$$

where the phase difference θ_j exceeds $\pi/2\,(\mathrm{mod}\,2\pi)$ and j is odd. These two equilibria belong to group I and group II, respectively.

In the following, we only focus on the type-1 saddle $\boldsymbol{T}_j^m$, the same results can be obtained for $\bar{\boldsymbol{T}}_j^m$.

The equations that determine the values of $\hat{\theta}_1^m$ and $\hat{\theta}_2^m$ are now (12a) (with $\hat{\theta}_i^m$ substituted for θ_i^m) combined with

$$\left(\frac{N}{2}-2\right)\hat{\theta}_1^m + \frac{N}{2}\hat{\theta}_2^m = (2m-1)\pi. \tag{22}$$

Hence, we find that the type-1 saddles are implicitly given as solutions of the following equation:

$$\sin\left(\hat{\theta}_1^m - \frac{(2m-1)\pi}{N} - \frac{2\hat{\theta}_1^m}{N}\right) = \frac{P}{2K\cos\left(\dfrac{(2m-1)\pi}{N} + \dfrac{2\hat{\theta}_1^m}{N}\right)}, \tag{23}$$

which admits a solution $\hat{\theta}_1^m \in [0, \frac{\pi}{2}]$ when $P/2K < \cos((2m-1)\pi/N + (2m+2\pi)/(N(N-2)))$. We next argue that the type-1 saddles found in Eq. (23) lie on the PEBS which surrounds the stable equilibrium $\boldsymbol{\theta}_S^m$. One could use the same arguments as previously invoked by DeVille.[14] In supplementary material Section S3, we provide a more general proof which is valid for different m.

We set $m = 0$ for the reasons described in Remark II in Section IV and denote $\boldsymbol{\theta}_S^0$ and $\boldsymbol{T}_j^0$ by $\boldsymbol{\theta}_S$ and $\boldsymbol{T}_j$, respectively. Note that there are $2N$ type-1 equilibria on the PEBS of $\boldsymbol{\theta}_S$ if

$P/2K$ is sufficiently large, and each line load is $P/2$ for the equilibrium $\boldsymbol{\theta}_S$ as shown in Fig. 3(a).

We proceed to calculate the potential energy differences (details given in supplementary material Section S4) between the stable state $\boldsymbol{\theta}_S$ and the saddle $\boldsymbol{T}_j$ for j odd, which we call ΔV_I

$$\begin{aligned}\Delta V_I = &-\frac{KN}{2}\left[\cos\hat{\theta}_1^0 - \cos\theta_1^0\right] - \frac{KN}{2}\left[\cos\hat{\theta}_2^0 - \cos\theta_2^0\right]\\ &+ 2K\cos\hat{\theta}_1^0 - \frac{NP}{4}\left[\hat{\theta}_1^0 - \theta_1^0\right] + \frac{NP}{4}\left[\hat{\theta}_2^0 - \theta_2^0\right]\\ &+\left(-\pi/2 + \hat{\theta}_1^0\right)P. \end{aligned} \tag{24}$$

We can recast Eq. (24), using Eq. (12a), in the following form:

$$\Delta V_I = P\left(-\frac{\pi}{2} + \arcsin\frac{P}{2K}\right) + \sqrt{4K^2 - P^2} + \Delta U_I, \tag{25}$$

where ΔU_I can be proven positive and has the asymptotic form for large N

$$\Delta U_I = \frac{1}{N}\left(\frac{\pi}{2} - \arcsin\frac{P}{2K}\right)^2\sqrt{4K^2 - P^2} + O(N^{-2}). \tag{26}$$

For $\bar{T}_j^0$, a similar calculation shows that the potential energy difference can be expressed as

$$\Delta V_{II} = P\left(\frac{\pi}{2} + \arcsin\frac{P}{2K}\right) + \sqrt{4K^2 - P^2} + \Delta U_{II}, \tag{27}$$

where ΔU_{II} can be proven positive and has the asymptotic form for large N

$$\Delta U_{II} = \frac{1}{N}\left(\frac{\pi}{2} + \arcsin\frac{P}{2K}\right)^2\sqrt{4K^2 - P^2} + O(N^{-2}). \tag{28}$$

We remark that for the case j is even, the derivation of the potential energy differences is analogous.

From the expression for the energy barriers ΔV_I and ΔV_{II}, we can easily infer that as the line load $\mathcal{L} = P/2$ increases, ΔV_1 decreases and ΔV_{II} increases. As mentioned before, ΔV_I is more susceptible to disturbances.

Furthermore, we can immediately draw the conclusion that for large network sizes, ΔV_I and ΔV_{II} approach a limiting value that depends only on K and P, which can be observed in Fig. 6(a). A direct calculation shows that the asymptotic limits correspond exactly to a potential difference found for a tree network, which is sketched in Fig. 3(b). Note that the line load of each line in the ring network and line 1 in the four nodes tree network are both $P/2$. Indeed, we find that for the line in a tree network with line load $P/2$, the energy leading it to desynchronization is ΔV_I^T and ΔV_{II}^T (Ref. 13)

$$\begin{aligned}\Delta V_I^T &= \frac{P}{2}\left(-\pi + 2\arcsin\frac{P}{2K}\right) + \sqrt{4K^2 - P^2},\\ \Delta V_{II}^T &= \frac{P}{2}\left(\pi + 2\arcsin\frac{P}{2K}\right) + \sqrt{4K^2 - P^2}. \end{aligned} \tag{29}$$

Hence, the energy barrier in Eqs. (25) and (27) can be explained in terms $\Delta V_I = \Delta V_I^T + \Delta U_I$ and $\Delta V_{II} = \Delta V_{II}^T + \Delta U_{II}$. As ΔU_I and ΔU_{II} are always positive, the energy needed to make a line lose synchronization (exceeding $\pi/2\,(\mathrm{mod}\,2\pi)$) is increased for the line in a ring network compared with in a tree network. In other words, the line with line load $\mathcal{L} = P/2$ in the ring network is more robust than in a tree network. This permits the line in cycles to transport

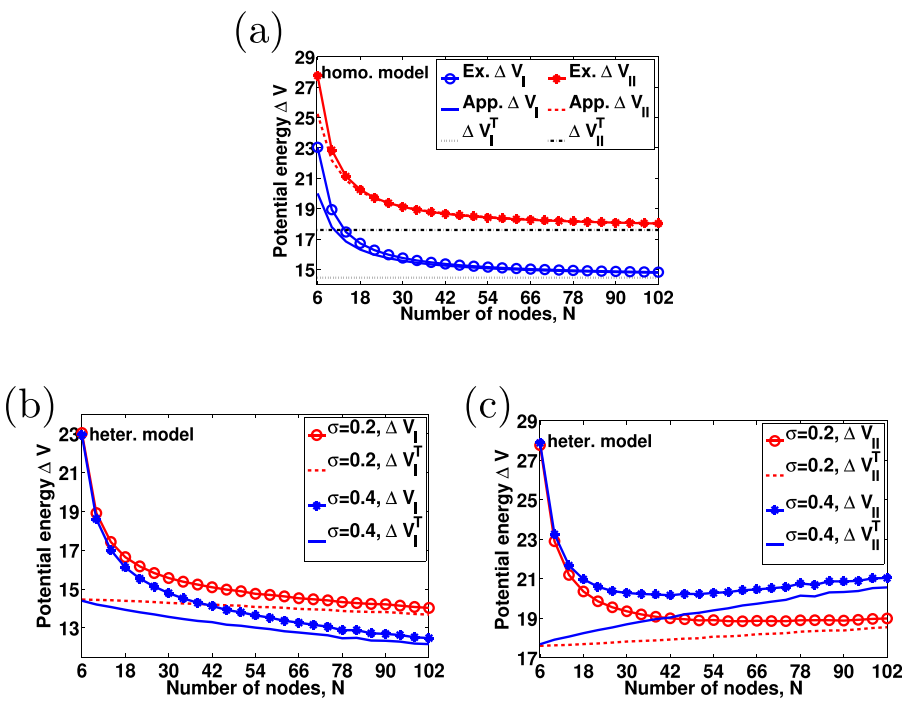

FIG. 6. (a) The potential energy ΔV_I, ΔV_{II}, ΔV_I^T and ΔV_{II}^T as functions of N for the homogeneous model. The approximate values of ΔV_I and ΔV_{II} are calculated neglecting the terms of $O(N^{-2})$ in Eqs. (26) and (28). (b) The average value of $\Delta V_I, \Delta V_I^T$ of the heterogeneous model as functions of N with $\sigma = 0.2, 0.4$. (c) The average value of $\Delta V_{II}, \Delta V_{II}^T$ of the heterogeneous model as functions of N with $\sigma = 0.2, 0.4$. $P = 1$ and $K = 8$ in all panels.

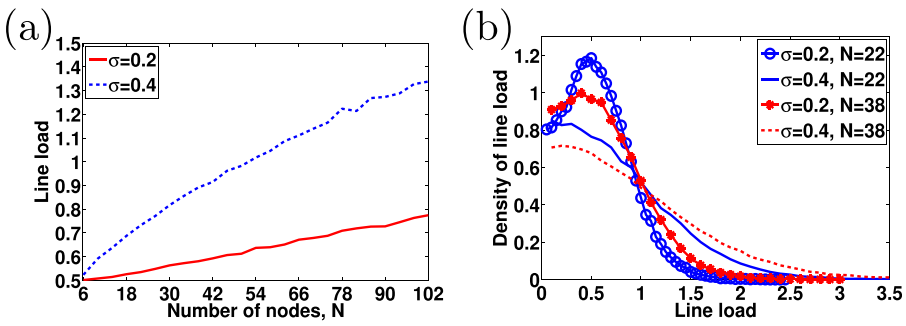

FIG. 7. (a) The average line load, calculated by Eq. (4), as a function of N for the heterogeneous model with $\sigma = 0.2, 0.4$. (b) The distribution of line loads of cyclic power grids with $N = 22, 38$ and $\sigma = 0.2, 0.4$. The distribution widens both for increasing values of N and σ. $P = 1$ and $K = 8$ in all panels.

more power. A ring topology results in an increased stability of the synchronous state compared to that of a tree network. This effect is larger for smaller networks. This finding corroborates the results by Menck *et al.*,[5] who found decreased stability from dead-ends or, small trees in the network.

In order to examine the robustness of our results, we next perform numerically studies on the heterogeneous model as in Eq. (5) with $\sigma > 0$.

B. Numerical results for the heterogeneous model

From the analysis of the nonlinear stability of cyclic power grids in the homogeneous model, we know that the potential energy differences between the type-1 equilibria and the stable synchronous state with $m = 0$ are always larger than the potential energy differences for a tree like network with the same line load $\mathcal{L}$. Moreover, the potential energy barrier of the ring network approaches that of the tree network as N increases. In the following, we verify whether this remains true for cyclic power grids with heterogeneous distribution of P_i and study how the heterogeneity of power distribution influences the nonlinear stability.

We next focus on how the potential energy of type-1 equilibria changes as N increases. As we remarked in Subsection V A, there are two groups of type-1 equilibria on the PEBS of $\boldsymbol{\theta}_S$, each having a different potential energy relative to the synchronous state, ΔV_I and ΔV_{II}, respectively.

As we do not have analytical expressions for ΔV_I and ΔV_{II} in this case, we numerically compute these values for different values of $\sigma > 0$ using the same procedure for assigning values to P_i as in Eq. (5). For different values of N, we perform 2000 runs to calculate ΔV_I and ΔV_{II} and compute the ensemble average. To determine which type-1 equilibria are on the PEBS of $\boldsymbol{\theta}_S$, the numerical algorithm proposed by Chiang *et al.*[35] is used.

Since σ is nonzero, incidentally a large value of P_i can be assigned to a node, which prevents the existence of a stable equilibrium. Such runs will not be considered in the average. Neither are runs in which fewer than $2N$ type-1 equilibria are found on the PEBS.

In our numerical experiments, we set again $K = 8, P = 1$, $P/K = 0.125$ and vary N between 6 and 102 and set either $\sigma = 0.4$ or $\sigma = 0.2$.

We determine the potential differences ΔV_I^T and ΔV_{II}^T by first calculating the stable equilibria $\boldsymbol{\theta}_S$. As $\boldsymbol{\theta}_S$ determines all phase differences, it facilitates computing the line loads by Eq. (4) between all connected nodes. From the line loads, we subsequently extract the value of P which we then substitute into Eq. (29) to find ΔV_I^T and ΔV_{II}^T, respectively.

By considering the average values of the quantities ΔV_I, ΔV_{II}, ΔV_I^T, ΔV_{II}^T, we conclude the following.

First, for the heterogeneous distribution of P_i, the average value of ΔV_I and ΔV_I^T decreases with N as shown in Figs. 6(b) and 6(c). This is because the average line load increases with N as shown in Fig. 7(a) and ΔV_I and ΔV_I^T are monotonously decreasing functions of the line load and N. However, ΔV_{II} decreases first and then increases after reaching a minimum with N since it is a monotonously increasing function of line load but a decreasing function of N. ΔV_{II}^T always increases since it is a monotonously increasing function of the line load.

Second, for larger σ, ΔV_I decreases faster and ΔV_{II} increases faster after reaching a minimum. Since ΔV_I determines the stability more than ΔV_{II}, the grid becomes less stable as σ increases. So cyclic power grids with a homogeneous distribution of P_i are more stable than ones with a heterogeneous distributed P_i.

Third, ΔV_I is lower bounded by ΔV_I^T and ΔV_{II} by ΔV_{II}^T, and converge to the respective bound as $N \to \infty$, which is consistent with the homogeneous case. This confirms that lines in a cyclic grid can withstand larger perturbations than corresponding lines in a tree network. As the size N of the cycle increases, this difference disappears gradually.

In order to get more insight into these scenarios, the distribution of $\Delta V_I, \Delta V_{II}, \Delta V_I^T$, and ΔV_{II}^T is plotted in Fig. 8 for different N and σ.

The distribution of ΔV_I and V_{II} converges to ΔV_I^T and ΔV_{II}^T, respectively, which can be observed from Figs. 8(a)–8(d). There is a boundary between ΔV_I and ΔV_{II} plotted by vertical black solid lines in the middle of Figs. 8(a)–8(f) for different sizes of networks. The boundary actually is the upper bound of ΔV_I and lower bound of ΔV_{II}, which is close to $2K + K\pi^2/2N$ calculated by setting $P = 0$ in Eq. (25) or (27). This does not depend on σ, as can be verified in Figs. 8(e) and 8(f). For the tree connection, the boundary of ΔV_I^T and ΔV_{II}^T plotted by vertical black dashed lines in the middle of Figs. 8(a)–8(d) equals $2K$ calculated by setting $P = 0$ in Eq. (29).

Figs. 8(e) and 8(f) show that the distribution of ΔV_I and ΔV_{II} becomes broader as either N or σ increases. This is also reflected in the distribution of the line loads shown in Fig. 7(b). We further remark that for the heterogeneous case, the line loads are different and the lines with smaller line load become stronger while the ones with larger line load become weaker. In other words, the power grid is more resilient

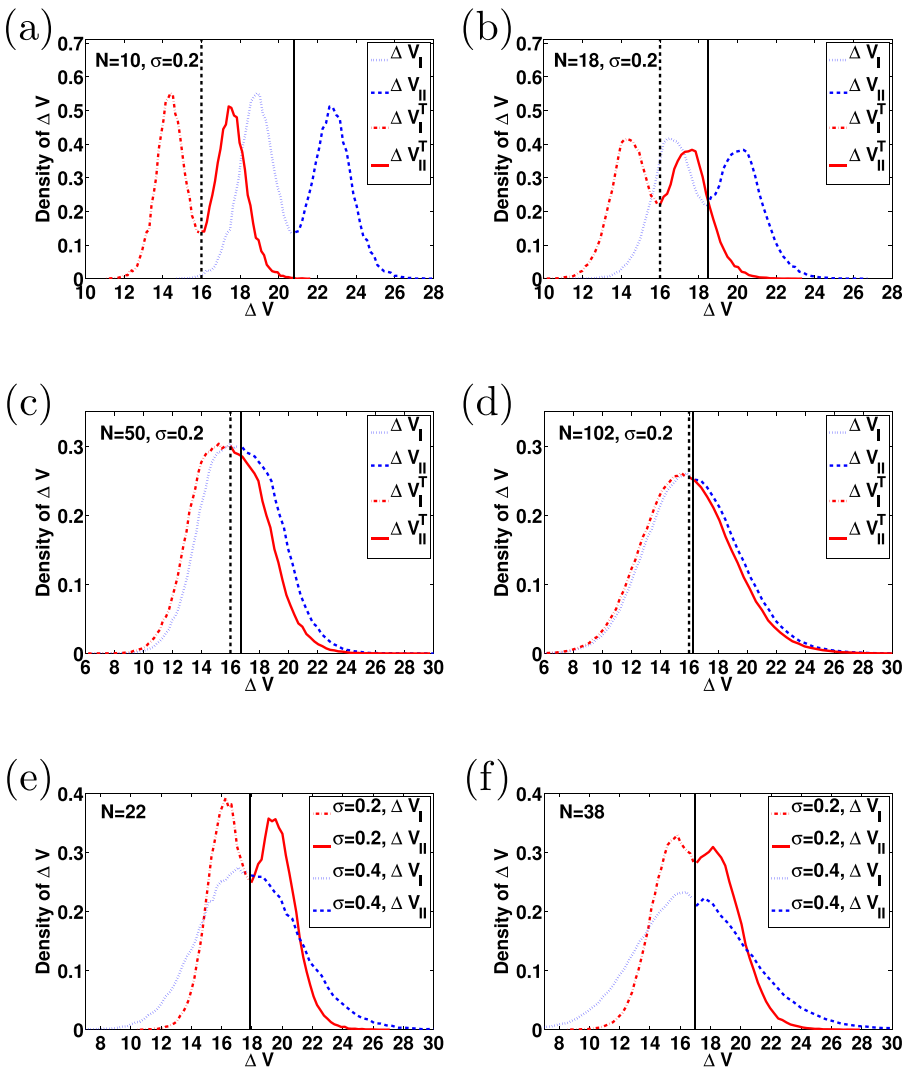

FIG. 8. (a)–(d) The distribution of ΔV_I, ΔV_{II}, ΔV_I^T and ΔV_{II}^T for cyclic power grids for $N = 10, 18, 50, 102$. (e) and (f) The distribution of ΔV_I and ΔV_{II} for $\sigma = 0.2$, 0.4 with $N = 22$, 38. The vertical black dashed lines in the middle of figures (a)–(d) denote the boundary between ΔV_I^T and ΔV_{II}^T and the vertical black solid lines in the middle of figures (a)–(f) indicate the boundary between ΔV_I and ΔV_{II}. $P = 1$ and $K = 8$ in all panels.

against some large disturbances while it is less resilient against others.

The maximum value of the density of potential energy is much smaller than that of the linear stability as shown in Figs. 4(c) and 4(d). This demonstrates that the potential energy is much more sensitive to the heterogeneity than the linear stability in the setting of P and K.

VI. CONCLUSION

Synchronous states and their stability in cyclic power grids have been studied in this paper. We derive analytical expressions for the stable equilibria of the cyclic power grids with homogeneous power distribution. Both linear and nonlinear stabilities are investigated for cyclic power grids. In particular, the nonlinear stability is measured by the energy barriers, which are the potential energy differences between the type-1 equilibria and the stable equilibrium. An analytical approximation of the energy barrier is obtained for the cyclic grids with a homogeneous distributed power generation and consumption. With an efficient algorithm for all the type-1 equilibria, numerical studies on the nonlinear stability have been performed for the cyclic power grids with heterogeneous distribution of power generation and consumption. For the homogeneous case, we find that adding cycles to the network increases the energy barriers. However, as the size of the cycle N approaches infinity, the energy barriers decrease to constants. For the heterogeneous case, the energy barrier decreases with both the heterogeneity and the size N. Therefore, to benefit from the increased stability of a ring like connection, the size of the cycle should not be too large (typically $N < 10$). Furthermore, for both homogeneous and heterogeneous cases, a line connecting two nodes in a ring network is more robust than a corresponding line in a tree network carrying the same line load.

An analytical approximation of the critical clearing time[39,40] of faults in power systems is derived by Roberts *et al.*,[41] which shows that larger potential energy of the closest equilibrium may increase the critical clearing time. The energy barrier measures the energy-absorbing capability of real power grids. In further study, it is worthwhile to investigate the energy barrier of small size artificial power grids to gain insight into improving the stability of the synchronous state of general power grids. However, the challenge remains to find all the type-1 equilibria of the power systems.

SUPPLEMENTARY MATERIAL

See supplementary material for the proof of Proposition III.1 and of Theorem IV.1 in Section S1, the algorithm for finding all the type-*j* equilibria in Section S2, the proof of the type-1 saddles in Eq. (23) being on the PEBS of $\boldsymbol{\theta}_S^m$ in Section S3, and the derivation of the energy barriers in Eqs. (25) and (26) in Section S4.

ACKNOWLEDGMENTS

We thank Jakob van der Woude for interesting conversations and comments during our regular meetings and we are extremely grateful to Jan H. van Schuppen for his interest, good suggestions and invaluable mathematical help. Kaihua Xi thanks the China Scholarship Council for financial support.

[1]S. Lozano, L. Buzna, and A. Díaz-Guilera, "Role of network topology in the synchronization of power systems," Eur. Phys. J. B **85**, 231 (2012).
[2]M. Rohden, A. Sorge, D. Witthaut, and M. Timme, "Impact of network topology on synchrony of oscillatory power grids," Chaos **24**, 013123 (2014).
[3]F. Dörfler and F. Bullo, "Synchronization in complex networks of phase oscillators: A survey," Automatica **50**, 1539–1564 (2014).
[4]A. Arenas, A. Díaz-Guilera, J. Kurths, Y. Moreno, and C. Zhou, "Synchronization in complex networks," Phys. Rep. **469**, 93–153 (2008).
[5]P. J. Menck, J. Heitzig, J. Kurths, and H. Joachim Schellnhuber, "How dead ends undermine power grid stability," Nat. Commun. **5**, 3969 (2014).
[6]D. Witthaut and M. Timme, "Braess's paradox in oscillator networks, desynchronization and power outage," New J. Phys. **14**, 083036 (2012).
[7]T. Coletta and P. Jacquod, "Linear stability and the Braess paradox in coupled-oscillator networks and electric power grids," Phys. Rev. E **93**, 032222 (2016).
[8]A. E. Motter, S. A. Myers, M. Anghel, and T. Nishikawa, "Spontaneous synchrony in power-grid networks," Nat. Phys. **9**, 191–197 (2013).
[9]L. M. Pecora and T. L. Carroll, "Master stability functions for synchronized coupled systems," Phys. Rev. Lett. **80**, 2109–2112 (1998).
[10]P. P. Varaiya, F. F. Wu, and R. L. Chen, "Direct methods for transient stability analysis of power systems: Recent results," Proc. IEEE **73**, 1703–1715 (1985).
[11]H. D. Chang, C. C. Chu, and G. Cauley, "Direct stability analysis of electric power systems using energy functions: Theory, applications, and perspective," Proc. IEEE **83**, 1497–1529 (1995).
[12]H. D. Chiang, F. F. Wu, and P. P. Varaiya, "Foundations of the potential energy boundary surface method for power system transient stability analysis," IEEE Trans. Circuits Syst. **35**, 712–728 (1988).
[13]H. D. Chiang, *Direct Methods for Stability Analysis of Electric Power Systems* (John Wiley & Sons, Inc., New Jersey, 2010).
[14]L. DeVille, "Transitions amongst synchronous solutions in the stochastic Kuramoto model," Nonlinearity **25**, 1473–1494 (2012).
[15]J. A. Lu, Y. Zhang, J. Chen, and J. Lu, "Scalability analysis of the synchronizability for ring or chain networks with dense clusters," J. Stat. Mech. Theory Exp. **2014**, P03008.
[16]P. Schultz, T. Peron, D. Eroglu, T. Stemler, G. M. Ramírez Ávila, F. A. Rodrigues, and J. Kurths, "Tweaking synchronization by connectivity modifications," Phys. Rev. E **93**, 062211 (2016).
[17]T. Nishikawa and A. E. Motter, "Synchronization is optimal in nondiagonalizable networks," Phys. Rev. E **73**, 065106 (2006).
[18]G. Filatrella, A. H. Nielsen, and N. F. Pedersen, "Analysis of a power grid using a Kuramoto-like model," Eur. Phys. J. B **61**, 485–491 (2008).
[19]M. Rohden, A. Sorge, M. Timme, and D. Witthaut, "Self-organized synchronization in decentralized power grids," Phys. Rev. Lett. **109**, 064101 (2012).
[20]A. R. Bergen and V. Vittal, *Power Systems Analysis*, 2nd ed. (Prentice-Hall Inc., New Jersey, 2000).
[21]J. Ochab and P. Góra, "Synchronization of coupled oscillators in a local one-dimensional Kuramoto model," Acta. Phys. Pol. B Proc. Suppl. **3**, 453–462 (2010).
[22]R. Delabays, T. Coletta, and P. Jacquod, "Multistability of phase-locking and topological winding numbers in locally coupled Kuramoto models on single-loop networks," J. Math. Phys. **57**, 032701 (2016).
[23]D. Mehta, N. S. Daleo, F. Dörfler, and J. D. Hauenstein, "Algebraic geometrization of the Kuramoto model: Equilibria and stability analysis," Chaos **25**, 053103 (2015).
[24]D. Mehta, H. D. Nguyen, and K. Turitsyn, "Numerical polynomial homotopy continuation method to locate all the power flow solutions," IET Gener. Transm. Distrib. **10**, 2972–2980 (2016).
[25]D. J. Bates, J. D. Hauenstein, A. J. Sommese, and C. W. Wampler, http://bertini.nd.edu for "Bertini: Software for Numerical Algebraic Geometry."
[26]L. A. Luxemburg and G. Huang, "On the number of unstable equilibria of a class of nonlinear systems," in *26th IEEE Conf. Decision Control* (IEEE, 1987), Vol. 20, pp. 889–894.
[27]J. Baillieul and C. Byrnes, "Geometric critical point analysis of lossless power system models," IEEE Trans. Circuits Syst. **29**, 724–737 (1982).
[28]J. C. Bronski and L. DeVille, "Spectral theory for dynamics on graphs containing attractive and repulsive interactions," SIAM J. Appl. Math. **74**, 83–105 (2014).
[29]S. H. Strogatz and R. E. Mirollo, "Collective synchronisation in lattices of nonlinear oscillators with randomness," J. Phys. A: Math. Gen. **21**, L699 (1988).
[30]J. Zaborszky, G. Huang, B. Zheng, and T. C. Leung, "On the phase portrait of a class of large nonlinear dynamic systems such as the power system," IEEE Trans. Autom. Control **33**, 4–15 (1988).
[31]J. A. Rogge and D. Aeyels, "Stability of phase locking in a ring of unidirectionally coupled oscillators," J. Phys. A: Math. Gen. **37**, 11135–11148 (2004).
[32]T. Coletta, R. Delabays, I. Adagideli, and P. Jacquod, "Topologically protected loop flows in high voltage ac power grids," New J. Phys. **18**, 103042 (2016).
[33]P. J. Menck, J. Heitzig, N. Marwan, and J. Kurths, "How basin stability complements the linear-stability paradigm," Nat. Phys. **9**, 89–92 (2013).
[34]F. Hellmmann, P. Schutz, C. Grabow, J. Heitzig, and J. Kurths, "Survivability of deterministic dynamical systems," Sci. Rep. **6**, 29654 (2016).
[35]H. D. Chiang, M. Hirsch, and F. Wu, "Stability regions of nonlinear autonomous dynamical systems," IEEE Trans. Autom. Control **33**, 16–27 (1988).
[36]J. Zaborsky, G. Huang, T. C. Leung, and B. Zheng, "Stability monitoring on the large electric power system," in *24th IEEE Conference on Decision Control* (IEEE, 1985), Vol. 24, pp. 787–798.
[37]C. W. Liu and J. S. Thorp, "A novel method to compute the closest unstable equilibrium point for transient stability region estimate in power systems," IEEE Trans. Circuits Syst. I, Fundam. Theory Appl. **44**, 630–635 (1997).
[38]J. Lee and H. D. Chiang, "A singular fixed-point homotopy methodtolocate the closest unstable equilibrium point for transient stability region estimate," IEEE Trans. Circuits Syst. II, Exp. Briefs **51**, 185–189 (2004).
[39]P. M. Anderson and A. A. Fouad, *Power System Control and Stability*, 2nd ed. (Wiley-IEEE Press, 2002).
[40]P. Kundur, *Power System Stability and Control* (McGraw-Hill, New York, 1994).
[41]L. G. W. Roberts, A. R. Champneys, K. R. W. Bell, and M. di Bernardo, "Analytical approximations of critical clearing time for parametric analysis of power system transient stability," IEEE J. Emerging Sel. Top. Circuits Syst. **5**, 465–476 (2015).